Pergamon

Int. J. Heat Mass Transfer. Vol. 38, No. 4, pp. 713–722, 1995

0017–9310/95 $9.50+0.00

0017–9310(94)00189–8

Effects of film vaporization on turbulent mixed convection heat and mass transfer in a vertical channel

WEI-MON YAN

Department of Mechanical Engineering, Hua Fan College of Humanities and Technology, Shih-Ting, Taipei, Taiwan 22305, R.O.C.

(*Received* 13 *September* 1993 *and in final form* 8 *June* 1994)

Abstract—Effects of combined buoyancy forces of thermal and mass diffusion on turbulent forced convection heat and mass transfer in downward flow were numerically examined in detail. Results are presented for air–water system under different conditions. Particular attention is paid to investigating the role of latent heat transport associated with the film vaporization in turbulent mixed convection heat and mass transfer. Predicted results show that the heat transfer along the gas–liquid interface is dominated by the latent heat transfer. The results also show that the assumption of an extremely thin film thickness made by Lin *et al.* [*J. Heat Transfer* **110,** 337–344 (1988)] is inappropriate, particularly for a system with a large liquid mass flow rate B. Additionally, it is found that the opposing-buoyancy forces would cause an enhancement in heat and mass transfer results compared with the corresponding results of forced convection. And the extent of enhancement in heat and mass transfer coefficients increases with the increase in T_w or q''_w.

1. INTRODUCTION

Systems in which both heat and mass are transferred include processes such as film cooling, cooling towers, heat recovery processes from waste hot water, crystal growth by physical or chemical vapor deposition, vapor deposition of thin films, and drying processes. Due to their widespread applications, heat and mass transfer between a flowing liquid film and an air stream has received considerable attention. Whereas a large number of investigations have been made concerning laminar heat and mass transfer problems, the study of turbulent mixed convection heat and mass transfer has not received adequate attention.

The aiding-buoyancy force on turbulent forced convection heat transfer in a vertical pipe was examined by Carr *et al.* [1] and Connor and Carr [2]. Their results showed that at high Grashof numbers a limiting profile shape was approached, with the maximum velocity shifting towards the heated wall. The effects of opposing-buoyancy force on the characteristics of flow and heat transfer in turbulent pipe flows were investigated by Axcell and Hall [3], Easby [4] and Khosla *et al.* [5]. They observed a marked enhancement in the heat transfer rate but a decrease in the friction coefficient compared with the corresponding results of turbulent forced convection. Turbulent mixed convection between vertical parallel plates subjected to different wall temperatures was investigated by Nakajima *et al.* [6]. In order to simulate the problem, they adopted a modified mixing length model to examine the effects of aiding and opposing buoyancy forces on fully-developed turbulent forced convection. Abdelmeguid and Spalding [7] applied, for the first time, a two-equation model for turbulent mixed convection pipe flows. Their model adopted a simple treatment near the wall, utilizing the wall function. Recently, Tanaka *et al.* [8], Cotton and Jackson [9] and Torii *et al.* [10] applied a low-Reynolds-number k–ε turbulent model to predict the turbulent mixed convection heat transfer and flow in vertical pipes. They were fairly successful in predicting heat transfer distribution with the experimental results.

Due to the complexity of couplings between the momentum, heat and mass transfer in the flow, early studies focused on heat and mass transfer in a gas stream by assuming the liquid film to be extremely thin. Under this assumption transport in the liquid film can be replaced by the approximate boundary conditions for gas flow. This type of analysis was carried out for forced convection heat and mass transfer over a flat plate [11–13] and a wedge [14]. A similar study was conducted by Chandra and Savery [15] for upward forced air over a falling isopropyl alcohol film by the integral method. As far as mixed convection heat and mass transfer is concerned, Yeh *et al.* [16] numerically examined the effects of heat and mass buoyancy forces on laminar forced convection heat transfer over a flat plate. Recently, Yan and his colleagues [17, 18] investigated the influences of wetted wall on laminar mixed convection heat and mass transfer in vertical ducts. The results show that the heat transfer enhancement through mass diffusion

NOMENCLATURE

b half channel width [m]
B liquid mass flow rate per unit periphery length at inlet
C_1, C_2, C_μ constants appearing in turbulent k–ε equations
c_p specific heat [J kg^{-1} K^{-1}]
c_{pa} specific heat for air [J kg^{-1} K^{-1}]
c_{pv} specific heat for water vapor [J kg^{-1} K^{-1}]
D mass diffusivity [m^2 s^{-1}]
D_h hydraulic diameter, $4b$ [m]
h_{fg} latent heat of vaporization [J kg^{-1}]
f_2, f_μ functions appearing in turbulent k–ε equations
g gravitational acceleration [m s^{-2}]
Gr_M Grashof number for mass transfer, $g(M_a/M_v-1)(w_I-w_o)D_e^3/v_o$
Gr_T Grashof number for heat transfer, $g\beta(T_w-T_o)D_e^3/v_o^2$ for UWT; $g\beta q''_w D_e^4/(v_o^2 k_o)$ for UHF
h_M mass transfer coefficient
k turbulent kinetic energy [m^2 s^{-2}]
$\dot{m}''_I$ evaporating mass flux [kg s^{-1} m^{-2}]
M_a molar mass of air [kg K^{-1} mol^{-1}]
M_v molar mass of vapor [kg K^{-1} mol^{-1}]
Nu_l local Nusselt number for latent heat transport, equation (18)
Nu_s local Nusselt number for sensible heat transport, equation (17)
Nu_x overall Nusselt number, equation (15), Nu_s+Nu_l
p_I partial pressure of water vapor at the gas–liquid interface [kPa]
Pr_t turbulent Prandtl number
p mixture pressure [kPa]
p_m motion pressure, $p-p_o$
Pr Prandtl number, v_o/α_o
q''_I total interfacial energy flux, equation (14) [W m^{-2}]
q''_{lI} latent heat flux (or net enthalpy flux), $\dot{m}''_I h_{fg}$ [W m^{-2}]
q''_{sI} sensible heat flux [W m^{-2}]
Re Reynolds number, $\bar{u}\cdot 4b/v_o$
R_t turbulent Reynolds number, $k^2/(v\varepsilon)$
Sc Schmidt number, v_o/D_o
Sh interfacial Sherwood number
T temperature [K, °C]
T_{li} inlet liquid film temperature [K, °C]
T_o inlet temperature [K, °C]
T_w wall temperature [K, °C]
u axial velocity [m s^{-1}]
u_f fully-developed velocity at inlet [m s^{-1}]
$\bar{u}_f$ average inlet velocity [m s^{-1}]
u_* shear stress velocity, $(\tau_w/\rho)^{1/2}$
v transverse velocity [m s^{-1}]
w mass fraction of water vapor
w_I mass fraction of water vapor at gas–liquid interface
x coordinate in the flow direction [m]
X dimensionless axial location, x/b
y coordinate in the transverse direction, m
y^+ dimensionless wall coordinate, $(b-y-\delta)\cdot u_*/v$.

Greek symbols

α thermal diffusivity [m^2 s^{-1}]
β coefficient of thermal expansion
δ local liquid film thickness [m]
ε the rate of dissipation of turbulent kinetic energy [m^2 s^{-3}]
λ molecular thermal conductivity [W m^{-1} °C^{-1}]
λ_t turbulent eddy conductivity [W m^{-1} °C^{-1}]
τ shear stress [kPa]
τ_I shear stress at the gas–liquid interface [kPa]
μ molecular dynamic viscosity [N s m^{-2}]
μ_t turbulent eddy viscosity [N s m^{-2}]
ρ density [kg m^{-3}]
ϕ relative humidity at inlet
σ_k turbulent Prandtl number for k
σ_ε turbulent Prandtl number for ε.

Subscripts

a of air
b bulk quantity
g mixture (air + water vapor)
I condition at gas–liquid interface
l liquid film
o condition at inlet
t turbulent
v of vapor
w condition at wall.

connected with liquid film vaporization is pronounced. However, their results are limited by the assumption that the liquid film on the wetted wall is negligibly thin. In practical situations, the liquid film on the wetted wall has a finite thickness, and thus the influences of the momentum and energy transports in the liquid film on the heat and mass transfer in the gas flow should be considered in the study.

The detailed analysis, including transport processes in the gas flow and liquid film, was simultaneously performed for turbulent gas flow over a vaporizing liquid film by Shembharkar and Pai [19] and Bau-

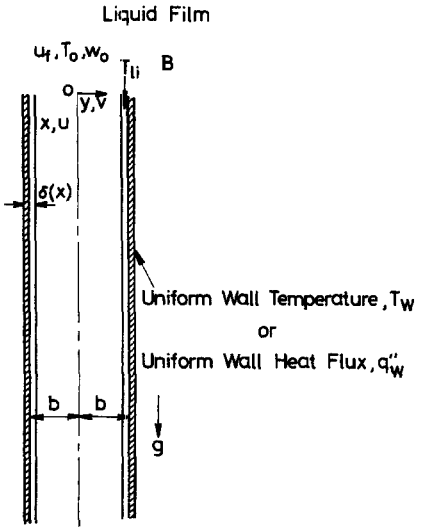

Fig. 1. Schematic diagram of the physical system.

mann and Thiele [20, 21]. In these studies the temperature distributions across the liquid film were assumed to be linear and buoyancy effects in the gas stream were not considered. Recently, laminar mixed convection heat and mass transfer in vertical ducts was explored by Yan [22, 23]. Often, in practical applications, heat and mass transfer over a vaporizing liquid film is always encountered in a turbulent convection flow. This motivates the present study which examines the turbulent convection heat and mass transfer with thermal and solutal buoyancy effects.

2. ANALYSIS

Partial filmwise evaporation of air–water mixtures is considered in a vertical channel with cocurrent downstream flow of both the gas stream and the falling liquid film (see Fig. 1). The thin liquid film is fed with an inlet liquid temperature T_{li} and inlet liquid mass flow rate B. The channel wall is maintained at either a constant wall temperature T_w or a prescribed uniform heat flux q''_w. The flow of moist air with relative humidity ϕ enters the channel from the top end with a fully-developed velocity u_f and uniform temperature T_o and concentration w_o. The interfacial heat and mass transfer is apparently determined by the coupled transport processes in the liquid film and gas stream. The liquid film evaporates into the gas stream as it flows downstream, and thus generates thermal and solutal buoyancy forces. Therefore, the forced gas flow is opposed and modified by these buoyancy forces along with the shearing effect created by the falling film. In this work, the effects of the coupled thermal and mass diffusion on the turbulent forced convection heat and mass transfer are examined in detail. Particular attention is paid to the investigation of the extent of the energy transport through mass diffusion, a latent heat exchange process, in comparison with that through thermal diffusion, a sensible heat transport process.

In the present study, a detailed numerical study was performed to investigate the turbulent mixed convection heat and mass transfer by simultaneously solving the conservation equations for various transport processes in the liquid film and gas stream with interfacial matching conditions. An attempt has been made here to model the process with the following simplifying assumptions:

1. The gas flow is a two-dimensional and boundary-layer type flow.
2. Radiation heat transfer, viscous dissipation and other secondary effects are negligible.
3. Consideration is given to a system with a low liquid mass flow rate and hence the liquid film flow is assumed to be laminar. In this study, the maximum mass flow rate for laminar liquid film flow is $B = 400\mu_l$ [24].
4. The inertia terms in the momentum equation of the liquid film are small compared with the viscous term [19–21].
5. The gas–liquid interface is in thermodynamic equilibrium.

2.1. *Governing equations*

With the above assumptions, the steady laminar momentum and heat transfer in the liquid film can be described by the following equations:

Axial-momentum equation

$$0 = \partial(\mu_l \partial u_l/\partial y)/\partial y + \rho_l g. \quad (1)$$

Energy equation

$$\rho_l c_{pl} u_l \partial T_l/\partial x = \partial(\lambda_l \partial T_l/\partial y)/\partial y. \quad (2)$$

Steady mixed convection heat and mass transfer in turbulent gas stream can be explored, with the usual boundary-layer approximations, by the following equations:

Continuity equation

$$\partial(\rho u)/\partial x + \partial(\rho v)/\partial y = 0. \quad (3)$$

Axial-momentum equation

$$\rho u \partial u/\partial x + \rho v \partial u/\partial y = -\mathrm{d}p_m/\mathrm{d}x + \partial[(\mu + \mu_t)\partial u/\partial y]/\partial y - (\rho_0 - \rho)g. \quad (4)$$

Energy equation

$$\rho c_p u \partial T/\partial x + \rho c_p v \partial T/\partial y = \partial[(\lambda + \lambda_t)\partial T/\partial y]/\partial y. \quad (5)$$

Concentration equation of water vapor

$$\rho u \partial w/\partial x + \rho v \partial w/\partial y = \partial[\rho(D + D_t)\partial w/\partial y]/\partial y. \quad (6)$$

It is noted in equation (4) that the third term on the right-hand side represents the buoyancy forces due to the variations in temperature and concentration.

In the study of steady convection channel flow, the overall mass balance at every axial location should be satisfied:

$$\int_0^{b-\delta} \rho_g u_g \, dy = \rho_0 \bar{u}_f (b-\delta_0) - \int_0^x \rho_g v_I \, dx. \quad (7)$$

This equation is used to deduce the pressure gradient in the gas flow.

2.2. *Boundary and interfacial conditions*

The two sets of governing equations, equations (1)–(6), are subjected to the following boundary conditions: at the channel wall the no-slip conditions for u- and v-velocities has to be satisfied as well as a constant wall temperature or a uniform wall heat flux. On the channel axis, all gradients in the mixture flow will be zero because of symmetry arguments. The inlet conditions are fully-developed velocity and flat temperature and concentration distributions.

The interfacial matching conditions specified at the gas–liquid interface, $y = b-\delta(x)$, are described as follows:

(1) continuity of velocity and temperature

$$u_I(x) = u_{g,I} = u_{l,I} \quad T_I(x) = T_{g,I} = T_{l,I} \quad (8)$$

(2) continuity of shear stress

$$\tau_I(x) = [(\mu+\mu_t)(\partial u/\partial y)]_{g,I} = (\mu \partial u/\partial y)_{l,I} \quad (9)$$

(3) vaporizing flux of water vapor into the gas flow

$$\dot{m}_I'' = -\rho v_I = \rho(D+D_t)/(1-w_I)\,\partial w/\partial y \quad (10)$$

(4) energy balance at the gas–liquid interface

$$(\lambda \partial T/\partial y)_{l,I} = [(\lambda+\lambda_t)(\partial T/\partial y)]_{g,I} + \dot{m}_I'' h_{fg}. \quad (11)$$

At the gas–liquid interface, the liquid film equations and the gas flow equations are coupled via boundary conditions (8)–(11). The interfacial water vapor concentration w_I and evaporating velocity v_I can be calculated once the temperature at the gas–liquid interface is known [24]:

$$w_I = M_v p_I/[M_a(p-p_I)+M_v p_I] \quad (12)$$

$$v_I = -[(D+D_t)/(1-w_I)](\partial w/\partial y)_I \quad (13)$$

where p and p_I are the local absolute pressure and the water vapor pressure at the interface, respectively. By assuming that the interface is in thermodynamic equilibrium, the relation between the saturated temperature and saturated pressure is described by the Clausius–Clapeyron equation. A convenient set of correlations for calculating the saturated pressure and latent heat at a saturated temperature was developed by Fujii *et al.* [25].

It is worth noting in equation (11) that the first and second terms on the right-hand side represent the interfacial heat flux from the interface to the gas stream, q_{sI}'', and the net enthalpy due to the latent heat transfer (film vaporization), q_{lI}'', respectively. The term on the left-hand side of equation (11) stands for the interfacial heat flux in the liquid side and is regarded as the interfacial heat flux, q_I''. Therefore, the interfacial heat flux from the interface to the gas stream can then be expressed as:

$$q_I'' = q_{sI}'' + q_{lI}'' = [(\lambda+\lambda_t)(\partial T/\partial y)]_{g,I} + \dot{m}_I'' h_{fg}. \quad (14)$$

The local Nusselt number along the gas–liquid interface, defined as:

$$Nu_x = h(4b)/\lambda_g = q_I''(4b)/[\lambda_g(T_I - T_b)] \quad (15)$$

can be written as:

$$Nu_x = Nu_s + Nu_l \quad (16)$$

where Nu_s and Nu_l are, respectively, the local Nusselt numbers for sensible and latent heat transfer, and are evaluated by:

$$Nu_s = q_{sI}''(4b)/[\lambda_g(T_I - T_b)] \quad (17)$$

and:

$$Nu_l = q_{lI}''(4b)/[\lambda_g(T_I - T_b)]. \quad (18)$$

Similarly, the local Sherwood number at the interface is defined as:

$$Sh = h_M(4b)/D = \dot{m}_I''(1-w_I)(4b)/[\rho_g D(w_I - w_b)]. \quad (19)$$

Note that in the above formulation the thermophysical properties of the gas mixture and liquid film are considered as variable with temperature and mixture composition. They are calculated from the pure component data by means of mixing rules [26, 27] applicable to any multicomponent mixtures. The pure component data [25] are approximated by polynomials in terms of temperature.

3. TURBULENCE MODELING

The turbulent viscosity μ_t is computed in accordance with k–ε turbulence model. Hence the transport equations for the turbulent kinetic and turbulent energy dissipation must be included in the analysis. To procure more reliable results, a modified low-Reynolds-number k–ε model developed by Myong *et al.* [28] and Myong and Kasagi [29] is adopted to eliminate the usage of wall functions in the computation and thus to permit direct integration of the transport equations to the gas–liquid interface. The equations of the modified low-Reynolds-number k–ε model are:

The turbulent kinetic energy equation

$$\rho u \partial k/\partial x + \rho v \partial k/\partial y = \partial[(\mu+\mu_t/\sigma_k)\partial k/\partial y]/\partial y + \mu_t(\partial u/\partial y)^2 - \rho\varepsilon. \quad (20)$$

The rate of dissipation of turbulent kinetic energy equation

$$\rho u \partial \varepsilon/\partial x + \rho v \partial \varepsilon/\partial y = \partial[(\mu+\mu_t/\sigma_\varepsilon)\partial \varepsilon/\partial y]/\partial y + C_1(\varepsilon/k)\mu_t(\partial u/\partial y)^2 - \rho C_2 f_2 \varepsilon^2/k \quad (21)$$

where:

$$\mu_t = \rho C_\mu f_\mu k^2/\varepsilon \quad (22)$$

$$f_2 = \{1-(2/9)\exp[-(R_t/6)^2]\}[1-\exp(-y^+/5)]^2 \quad (23)$$

$$f_\mu = (1+3.45/\sqrt{R_t})[1-\exp(-y^+/70)] \quad (24)$$

$$R_t = k^2/(\nu\varepsilon) \quad y^+ = (b-y-\delta)u_*/\nu \quad u_* = (\tau_w/\rho)^{1/2} \quad (25)$$

$$\sigma_k = 1.4 \quad \sigma_\varepsilon = 1.3$$

$$C_1 = 1.4 \quad C_2 = 1.8 \quad C_\mu = 0.09. \quad (26)$$

As the flow includes heat and mass transfer, turbulent Prandtl and Schmidt numbers must be specified. Analogy between heat and mass transfer is assumed. Simpson *et al.* [30] determined the turbulent Prandtl number for air from measurements. Their results indicate no appreciable effect of mass transfer on the turbulent Prandtl number. From the experimental investigations of Meier and Rotta [31] it is evident that the turbulent Prandtl number varies across the boundary layer. However, calculations of Cebeci [32], with a constant value $Pr_t = 0.9$ throughout the boundary layer, show no pronounced effect on Stanton number and temperature distributions. Therefore, this value will be used for all calculations.

4. SOLUTION METHOD

Discretization of the governing equation sets is performed by an implicit finite-difference scheme and the discretized equations are solved using a marching solution procedure. Correction of the pressure gradient and axial velocity profile at each axial station in order to satisfy overall continuity is achieved by using a method described by Anderson *et al.* [33]. In the present study the matching conditions imposed at the gas–liquid interface, equations (9) and (11), are cast in backward difference for $(\partial\psi/\partial y)_g$ and forward difference for $(\partial\psi/\partial y)_l$ with ψ denoting u or T. Therefore, the governing equations in the gas flow and liquid film can be solved simultaneously. The discretized governing equations form a set of tridiagonal matrix equation, which can be efficiently solved by the Thomas algorithm [34].

The change in film thickness in the flow direction due to the film evaporation process is considered in the present study. In the numerical computation, the grid lines were nonuniformly spaced to capture steep gradients of velocity, temperature and concentration near the channel entrance and in the vicinity of gas–liquid interface. During the program tests, solutions for a typical case were obtained using different grid sizes to ensure that the solution is grid-independent. The results from the computation for various grids are given in Table 1. It was noted that the differences in the local interfacial Nusselt number, Nu_x, from computations using either $201\times151\times31$ or $101\times101\times21$ grids were always within 2%. To reduce the cost of computation, the $101\times101\times21$ grid was chosen for subsequent computations. To further check the adequacy of the numerical scheme, computations were first carried out for the limiting case of laminar mixed convection heat and mass transfer in a vertical channel. The predicted results were compared with those of Yan [22]. Excellent agreement between present predictions and those of Yan [22] was found. Moreover, the results for the limiting case of turbulent mixed convection heat transfer in a vertical pipe was obtained first. The predicted results agree well with those of refs. [8, 9]. In view of these validations, the present numerical algorithm and employed grid layout are adequate to obtain accurate results for practical purposes.

5. RESULTS AND DISCUSSION

In view of the large number of parameters and of the extreme demands of the computational task, a full parametric exploration is unrealistic. Rather, the parameters were varied systematically in order to examine the key trends in the results. In light of practical situations, the following conditions are selected in the computations: unsaturated moist air with relative humidity $\phi = 50\%$ at 20°C and 1 atm enters a long vertical channel with half channel width $b = 0.04$ m

Table 1. Comparisons of local interfacial Nusselt number Nu_x for various grid arrangements for $T_w = 50$°C, $Re = 2\times10^4$, and $B = 0.02$ kg m^{-1} s^{-1}

	$I\times J\times K$				
X	$201\times151\times31$	$101\times151\times31$	$101\times101\times21$	$51\times101\times21$	$51\times51\times11$
2.10	648.15	647.66	649.60	665.01	618.94
5.26	540.58	540.18	541.87	545.22	514.53
10.10	490.86	491.31	492.88	494.10	467.98
15.50	469.08	469.37	470.78	472.09	447.32
20.10	459.65	459.93	461.44	462.12	438.82
40.84	450.10	450.16	451.68	451.93	427.79
60.0	450.17	450.14	451.58	451.50	427.46

I: total grid points placed in the longitudinal direction.
J: total grid points placed in the transverse direction in the gas side.
K: total grid points placed in the transverse direction in the liquid side.

Table 2. Values of major parameters for various cases (UWT)

Case	T_o (°C)	T_w (°C)	B (kg m^{-1} s^{-1})	Re	Gr_T	Gr_M	Pr	Sc	ϕ (%)
I	20	30	0.02	2×10^4	6.07×10^6	2.08×10^6	0.709	0.597	50
II	20	50	0.02	2×10^4	1.82×10^7	7.80×10^6	0.709	0.597	50
III	20	70	0.02	2×10^4	3.03×10^7	2.26×10^7	0.709	0.597	50
IV	20	50	0.01	2×10^4	1.82×10^7	7.80×10^6	0.709	0.597	50
V	20	50	0.04	2×10^4	1.82×10^7	7.80×10^6	0.709	0.597	50
VI	20	50	0.02	1×10^4	1.82×10^7	7.80×10^6	0.709	0.597	50
VII	20	50	0.02	5×10^4	1.82×10^7	7.80×10^6	0.709	0.597	50

Table 3. Values of major parameters for various cases (UHF)

Case	T_o (°C)	q''_w (W m^{-2})	B (kg m^{-1} s^{-1})	Re	Gr_T	Pr	Sc	ϕ (%)
I	20	1000	0.02	2×10^4	3.76×10^9	0.709	0.597	50
II	20	1500	0.02	2×10^4	5.65×10^9	0.709	0.597	50
III	20	2000	0.02	2×10^4	7.53×10^9	0.709	0.597	50

from the top by the combined action of certain external force as well as the buoyancy forces of thermal and mass diffusion. In this work, both the thermal and mass buoyancy forces act in the upward direction. Thus, the combined buoyancy forces oppose the flow of the gas stream. Results are obtained for several cases indicated in Tables 2 and 3.

5.1. *Uniform wall temperature*

To study the relative contributions of heat transfer through sensible and latent heat exchanges in the flow, both sensible heat Nusselt number Nu_s and latent heat Nusselt number Nu_l are presented in Fig. 2(a) and (b) with the wall temperature T_w as a parameter. For comparison purposes, the corresponding results without buoyancy effects (i.e. forced convection results) are also included in Fig. 2, as shown by the dashed curves. In Fig. 2, the buoyancy effect is negligible up to a certain axial distance X depending on the T_w. The higher T_w is, the shorter this distance is. After this onset point, the curve branches out from the corresponding results of forced convection. An overall inspection on Fig. 2(a) reveals that, near the entrance, a smaller Nu_s is noted for a higher T_w due to a greater evaporating (blowing) effect. Additionally, the heat transfer enhancement due to the opposing buoyancy forces, which can be identified by the vertical separation between the solid line and dashed line, increases with the increase in T_w. This stems from the fact that larger opposing forces are noted for a system with a higher T_w, and the retarding buoyancy forces would modify the turbulent flow to such an extent that both turbulent shear stress and turbulent energy transport are increased, leading to an augmentation in heat transfer. The effects of wetted wall temperature on the latent heat Nusselt number Nu_l are illustrated in Fig. 2(b). The flow with a higher T_w shows a larger Nu_l. This is brought about by the larger latent heat transport in connection with the larger liquid film evaporation for a higher T_w. It becomes apparent, by comparing the magnitudes of Nu_s and Nu_l, that heat transfer resulting from the latent heat exchange is much more effective. In Fig. 2(c), Nu_x, the sum of Nu_l and Nu_s, is presented.

The effects of wall temperature T_w on the local Sherwood number distributions are presented in Fig. 3(a). In this plot, a larger mass transfer enhancement, identified by the vertical separation between the solid

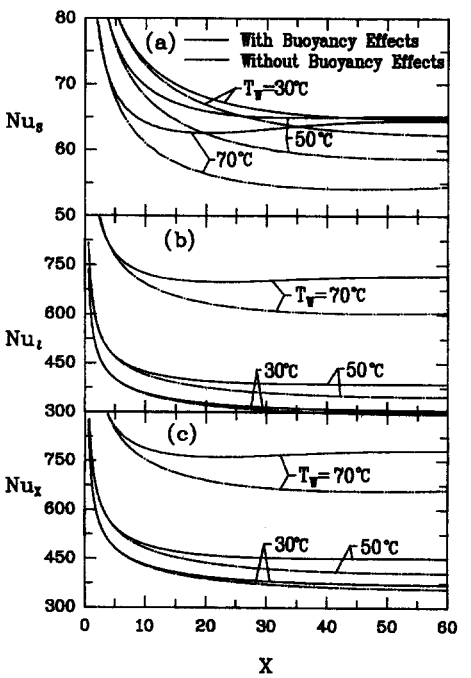

Fig. 2. Effects of wall temperature T_w on the local Nusselt numbers for (a) sensible heat; (b) latent heat; (c) overall at $B = 0.02$ kg m^{-1} s^{-1} and $Re = 2\times10^4$.

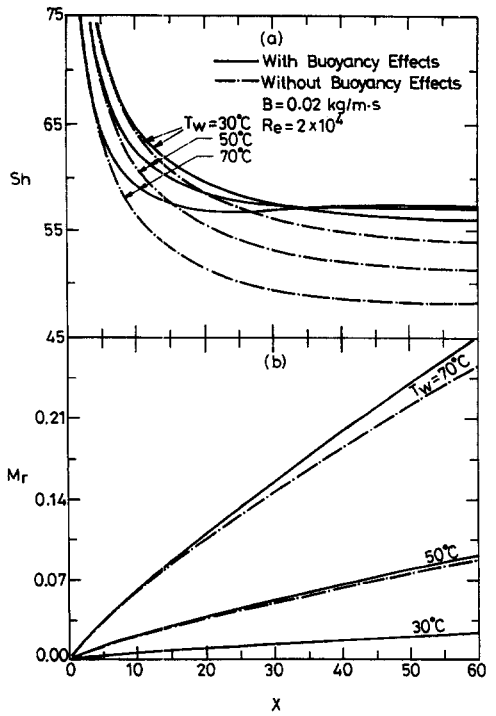

Fig. 3. Effects of wall temperature T_w on the local Sherwood number Sh and dimensionless accumulated evaporated rate M_1.

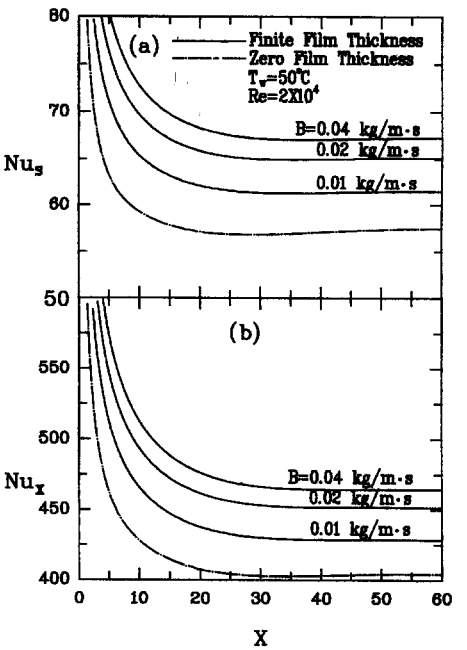

Fig. 4. Effects of inlet mass flow rate B on the local Nu_s and Nu_x.

line and dashed line, is found for a higher T_w (i.e. higher opposing-buoyancy forces). This is similar to the general concept that for turbulent mixed convection heat transfer, the heat transfer enhancement increases with the buoyancy forces in buoyancy-opposing flow.

The amount of water vapor added to the gas stream due to film evaporation is important in improving our understanding of heat and mass transfer processes. Additionally, the consumption of the liquid water due to the film vaporization is of interest in engineering applications. To meet these ends, a nondimensional accumulated mass evaporation rate is introduced:

$$M_r = \frac{\text{evaporating mass flow rate}}{\text{inlet liquid mass flow rate}} = \int_0^x \dot{m}_i'' \, dx/B. \tag{27}$$

The distributions of M_r for various T_w are presented in Fig. 3(b). For a rise in wall temperature T_w, a stronger film vaporization results, owing simply to the associated increase in T_I and w_I. It is worth noting that the largest M_r at $X = 60$ is about 28% for $T_w = 70°C$.

Comparisons are made in Figs. 4 and 5(a) to check the suitability of the assumption of an extremely thin film made by Lin *et al.* [17] in the analysis by examining the axial distributions of Nu_s, Nu_x and Sh predicted by including the transport in the finite liquid film and by ignoring it for the cases with $T_w = 50°C$ and $Re = 2 \times 10^4$ at a different liquid mass flow rate B. It is apparent that the Nu_s, Nu_x and Sh calculated with zero film thickness are smaller than those calculated with the finite film thickness. Besides, the differences between these two treatments increase with the liquid mass flow rate B. This implies that the assumption of an extremely thin film is only valid for a system with a small liquid mass flow rate B. But as

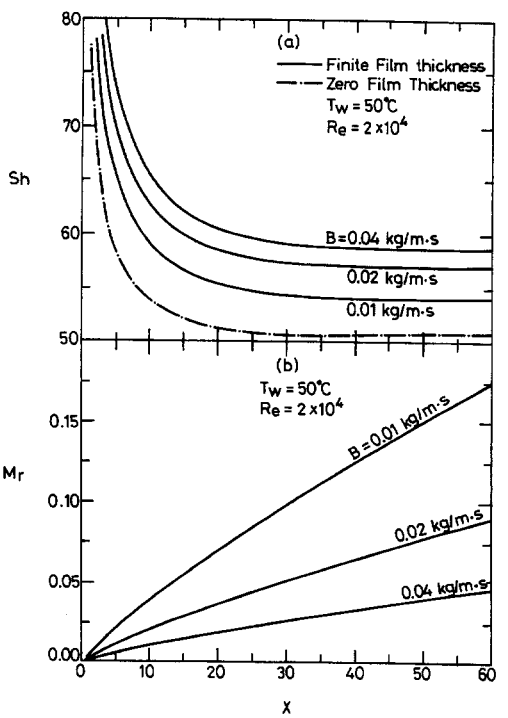

Fig. 5. Effects of inlet mass flow rate B on the local Sh and M_1.

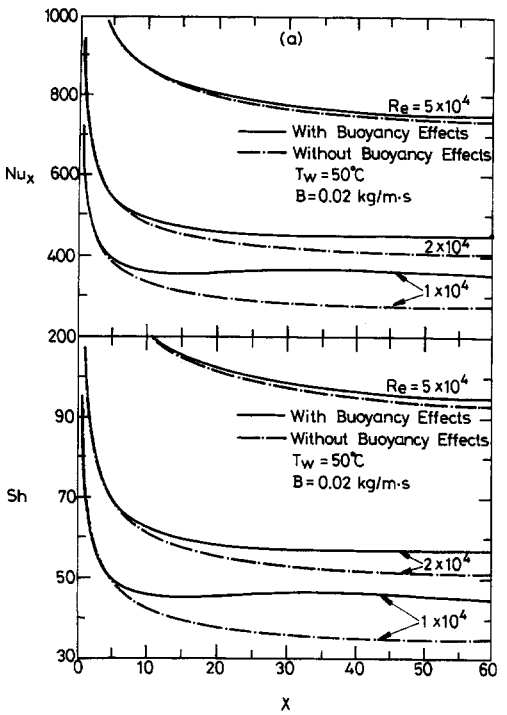

Fig. 6. Effect of Reynolds number Re on the local Nu_x and Sh.

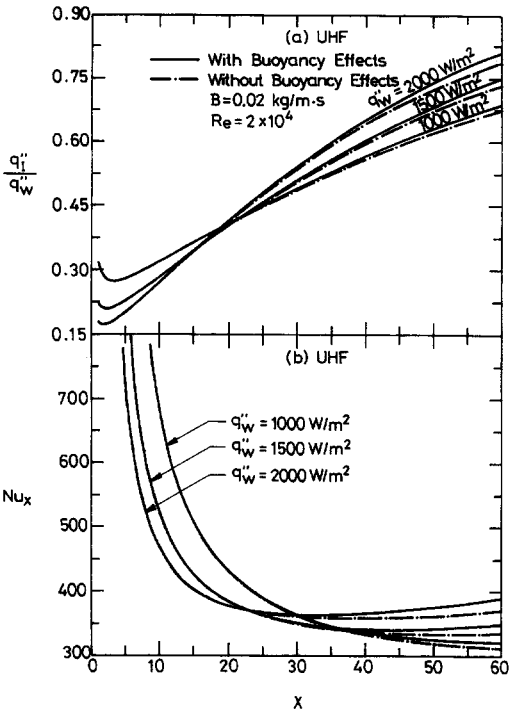

Fig. 7. Effects of wall heat flux q''_w on the local q''_l/q_w and Nu_x for uniform wall heat flux.

the liquid mass flow rate is large, the assumption can produce considerable error.

Figure 5(b) presents the effects of liquid mass flow rate B on the distributions of M_r. It is clear that a reduction in B causes a larger M_r. The largest M_r is about 17% for $B = 0.01\text{kg m}^{-1}\text{ s}^{-1}$.

The effects of Reynolds number Re on the axial distributions of Nu_x and Sh are shown in Fig. 6. It is clear that larger Nu_x and Sh are noted for a system with a higher Re. This confirms the general concept that, for turbulent forced convection, the heat transfer is larger for a higher Re. Additionally, the differences between the solid line and dashed line decrease with the increase in Re. This is due to the fact that the buoyancy effects decrease with the increase in Re.

5.2. *Uniform heat flux*

In this section solutions for uniform heat flux boundary conditions are presented. The local distributions of dimensionless interfacial heat flux q''_l/q''_w and Nusselt number Nu_x are depicted in Fig. 7(a) and (b), respectively. Figure 7(a) shows that near the entrance ($X < 15$) a larger q''_l/q''_w results for a lower wall heat flux q''_w. But as the flow goes downstream ($X > 25$) the reverse trend is noted. Also found in Fig. 7(a) are the effects of buoyancy forces. It is clear that, by comparing the solid line and dashed line, buoyancy effects are more significant at the downstream region and for a system with a higher q''_w. In Fig. 7(b), near the entrance, a larger q''_w shows a larger Nu_x. However, the result is reversed in the downstream direction.

The distributions of the interfacial mass evaporation rate and Sherwood number are presented in Fig. 8 for various q''_w to illustrate the mass transfer characteristics. In Fig. 8(a), an increase in the wall heat flux causes a greater film evaporation and $\dot{m}''_l$

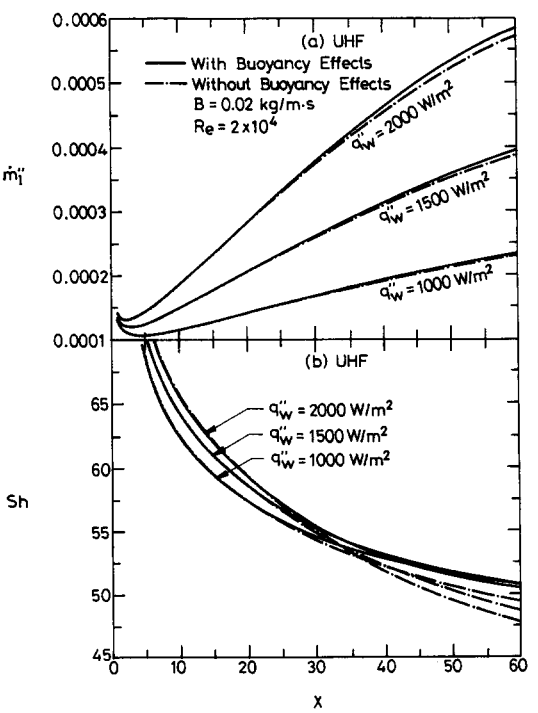

Fig. 8. Effects of wall heat flux q''_w on the local $\dot{m}''_l$ and Sh for uniform wall heat flux.

increases with X in the downstream region. These outcomes apparently result from the higher interfacial temperature T_I at a larger q''_w. The change in the wall heat flux has a smaller influence on the Sherwood number variations, as is evident from Fig. 8(b). Additionally, a larger mass transfer enhancement due to the opposing-buoyancy forces, identified by the vertical separation between the solid line and dashed line, is noted for a larger q''_w.

6. CONCLUSIONS

The characteristics of turbulent mixed convection heat and mass transfer in a wetted channel have been studied. The influences of wall heating conditions, inlet liquid mass flow rate, and Reynolds number on the characteristics of momentum, heat and species in the opposing flows were examined in detail. A brief summary of the major results is:

1. Opposing-buoyancy forces cause an enhancement in turbulent heat and mass transfer. The extent of the augmentation increases with the increase in T_w or q''_w (i.e. opposing-buoyancy forces), compared with the corresponding results of turbulent forced convection.
2. Heat transfer along the gas–liquid interface is dominated by the transport of latent heat in association with the vaporization of a liquid film.
3. The assumption of an extremely thin film thickness is valid only for a low liquid mass flow rate B. However, for a high liquid mass flow rate, the assumption introduces considerable error.
4. At the downstream region, larger dimensionless interfacial heat flux q''_I/q''_w and local Nu_x result for the system with a larger q''_w.

Acknowledgement—Financial support of this work by the National Science Council, R.O.C., through the contract NSC 82-0401-E211-003, is greatly appreciated.

REFERENCES

1. A. D. Carr, M. A. Connor and H. O. Buhr, Velocity, temperature, and turbulence measurement in air for pipe flow with combined free and forced convection, *J. Heat Transfer* **95,** 445–452 (1973).
2. M. A. Connor and A. D. Carr, Heat transfer in vertical tubes under conditions of mixed free and forced convection, *Sixth International Heat Transfer Conference*, Toronto, Canada, Vol. 2, pp. 43–48 (1978).
3. B. P. Axcell and W. B. Hall, Mixed convection to air in a vertical pipe, *Sixth International Heat Transfer Conference*, Toronto, Canada, Vol. 2, pp. 37–42 (1978).
4. J. P. Easby, The effect of buoyancy on flow and heat transfer for a gas passing down a vertical pipe at low turbulent Reynolds number, *Int. J. Heat Mass Transfer* **21,** 791–801 (1978).
5. J. Khosla, T. W. Hoffman and K. G. Pollock, Combined forced and natural convection heat transfer to air in a vertical tube, *Fifth International Heat Transfer Conference*, Tokyo, Japan, Vol. 3, pp. 144–148 (1974).
6. M. Nakajima, K. Fukui, H. Ueda and T. Mizushinal, Buoyancy effects on turbulent transport in combined free and forced convection between vertical parallel plates, *Int. J. Heat Mass Transfer* **23,** 1325–1336 (1980).
7. A. M. Abdelmeguid and D. B. Spalding, Turbulent flow and heat transfer in pipe with buoyancy effects, *J. Fluid Mech.* **94,** 383–400 (1979).
8. H. Tanaka, S. Maruyama and S. Hatano, Combined forced and natural convection heat transfer for upward flow in a uniformly heated, vertical pipe, *Int. J. Heat Mass Transfer* **30,** 165–174 (1987).
9. M. A. Cotton and J. D. Jackson, Vertical tube air flows in the turbulent mixed convection regime calculated using a low-Reynolds-number k–ε model, *Int. J. Heat Mass Transfer* **33,** 275–286 (1990).
10. S. Torii, A. Shimizu, S. Hasegawa and M. Higasa, Laminarization of strongly heated gas flows in a circular tube (numerical analysis by mean of a modified k–ε model), *JSME Int. J.* **33,** Ser. II, 538–547 (1990).
11. L. C. Chow and J. N. Chung, Evaporation of water into a laminar stream of air and superheated steam, *Int. J. Heat Mass Transfer* **26,** 373–380 (1983).
12. L. C. Chow and J. N. Chung, Water evaporation into a turbulent stream of air, humid air or superheated steam, *Twenty-first ASME/AIChE National Heat Transfer Conference*, Seattle, WA, ASME Paper No.83-HT-2 (1983).
13. J. Schroppel and F. Thiele, On the calculation of momentum, heat and mass transfer in laminar and turbulent boundary layer flows along a vaporizing liquid film, *Numer. Heat Transfer* **6,** 475–496 (1983).
14. C. H. Wu, D. C. Davis, J. N. Chung and L. C. Chow, Simulation of wedge-shaped product dehydration using mixtures of superheated steam and air in laminar flow, *Numer. Heat Transfer* **11,** 109–123 (1987).
15. V. Chandra and C. W. Savery, Forced convection heat and mass transfer from a falling film to a laminar external boundary layer, *Int. J. Heat Mass Transfer* **17,** 1549–1557 (1974).
16. Y. M. Yeh, S. W. Tsai and C. C. Yang, Heat and mass transfer in mixed convection over a horizontal plate, *Numer. Heat Transfer* **12,** 229–242 (1987).
17. T. F. Lin, C. J. Chang and W. M. Yan, Analysis of combined buoyancy effects of thermal and mass diffusion on laminar forced convection heat transfer in a vertical tube, *J. Heat Transfer* **110,** 337–344 (1988).
18. W. M. Yan, Mixed convection heat transfer enhancement through latent heat transport in vertical parallel plate channel flows, *Can. J. Chem. Engng* **69,** 1277–1282 (1991).
19. T. R. Shembharkar and B. R. Pai, Prediction of film cooling with a liquid coolant, *Int. J. Heat Mass Transfer* **29,** 899–908 (1986).
20. W. W. Baumann and F. Thiele, Heat and mass transfer in two-component film evaporation in a vertical tube, *Eighth International Heat Transfer Conference*, Vol. 5, pp. 1843–1848 (1986).
21. W. W. Baumann and F. Thiele, Heat and mass transfer in evaporating two-component liquid film flow, *Int. J. Heat Mass Transfer* **33,** 267–273 (1990).
22. W. M. Yan, Effects of film evaporation on laminar mixed convection heat and mass transfer in a vertical channel, *Int. J. Heat Mass Transfer* **35,** 3419–3429 (1992).
23. W. M. Yan, Binary diffusion and heat transfer in mixed convection pipe flows with film evaporation, *Int. J. Heat Mass Transfer* **36,** 2115–2123 (1993).
24. E. R. G. Eckert and R. M. Drake, Jr, *Analysis of Heat and Mass Transfer*, Chaps. 20 and 22. McGraw-Hill, New York (1972).
25. T. Fujii, Y. Kato and K. Bihara, Expressions of transport and thermodynamic properties of air, steam, and water, Sei San Ka Gaku Ken Kyu Jo., Report No. 66, Kyu Shu University, Kyu Shu, Japan (1977).

26. R. B. Bird, W. E. Stewart and E. N. Lightfoot, *Transport Phenomena*. Wiley, New York (1960).
27. R. C. Reid, J. M. Prausnitz and T. K. Sherwood, *The Properties of Gas and Liquid*, Chap. 11. Hemisphere/McGraw-Hill, New York (1977).
28. H. K. Myong, N. Kasagi and M. Hira, Numerical prediction of turbulent pipe flow heat transfer for various Prandtl number fluids with the improved k–ε turbulence model, *JSME Int. J.* **32,** 613–622 (1989).
29. H. K. Myong and N. Kasagi, A new approach to the improvement of k–ε turbulence model for wall bounded shear flow, *JSME Int. J.* **33,** 63–72 (1990).
30. R. L. Simpson, D. C. Whitten and R. J. Moffat, An experimental study of the turbulent Prandtl number of air with injection and suction, *Int. J. Heat Mass Transfer* **13,** 125–143 (1970).
31. H. U. Meier and J. C. Cotta, Temperature distributions in supersonic turbulent boundary layers, *AIAA J.* **9,** 2149–2156 (1971).
32. T. Cebeci, Eddy viscosity distribution in thick axisymmetric turbulent boundary layers, *J. Fluids Engng* **95,** 319–326 (1973).
33. D. A. Anderson, J. C. Tannehil and R. H. Pletcher, *Computation Fluid Mechanics and Heat Transfer*, Chap. 7. Hemisphere/McGraw-Hill, New York (1984).
34. R. S. Varga, *Matrix Iterative Analysis*. Prentice-Hall, Englewood Cliffs, NY (1962).